Solar Energy 230 (2021) 10–12

Contents lists available at ScienceDirect

Solar Energy

journal homepage: www.elsevier.com/locate/solener

# Conductivity of $Sb_xSe_y$ films grown by CMBD from Sb and Se precursors for use in solar cells

T.M. Razykov [a,*], A. Bosio [b], B.A. Ergahsev [a], D. Isakov [a], R. Khurramov [a], K.M. Kouchkarov [a], A. Romeo [c], N. Romeo [b], M.S. Tivanov [d]

[a] Physical-Technical Institute, Chingiz Aytmatov Street 2B, Tashkent 100084, Uzbekistan
[b] University of Parma, G.P Usberti 7/A, 43124 Parma, Italy
[c] Universita' di Verona, Ca' Vignal 2- Strada Le Grazie 15, 37134 Verona, Italy
[d] Faculty of Physics, Belarusian State University, 220030 Minsk, Belarus

ARTICLE INFO

*Keywords:*
Thin film
$Sb_2Se_3$
Chemical molecular beam deposition
Sb/Se ratio
Conductivity

ABSTRACT

Antimony selenide ($Sb_2Se_3$) has been developed as attractive, non-toxic and earth-abundant solar absorber candidate among the thin-film photovoltaic devices. The growth of $Sb_xSe_y$ thin films, by atmospheric pressure chemical molecular beam deposition (CMBD) method, from separate Sb and Se precursors has been reported. The conductivity of the films was investigated as a function of the vapor phase mixture of Sb and Se. By the precise control of the Sb/Se ratio we succeeded in obtaining stoichiometric $Sb_2Se_3$ films. It is also found out that we can control the conductivity by deliberately introducing the deviation from the stoichiometry. The conductivity was varied in the wide range of $10^{-5} \div 10^{2}$ (Ohm × cm)$^{-1}$ and samples had p- and n-type conductivity depending on Sb/Se ratio. The obtained results were explained by the formation of intrinsic point defects.

## 1. Introduction

Today, world researchers pay special attention to the use of $Sb_2Se_3$ layers as an absorbing layer for thin film solar cells (Mavlonov et al., 2020; Hongwey et al., 2019; Mamta et al., 2021). This is due to the fact that the physical properties of this material (p-type conductivity, band gap Eg = 1.01–1.2 eV, high absorption coefficient $\alpha > 10^5$ cm$^{-1}$, low melting point and high partial pressure) makes it possible to grow high-quality films at low temperatures (Mavlonov et al., 2020). In addition, the elements included in these materials have a relatively low cost (abundance in nature), stability under external influences and non-toxicity (Zhou et al., 2014). This will make it possible to manufacture environmentally friendly and efficient solar modules, as well as open the way for their wide production on an industrial scale.

Currently, the efficiency of thin-film solar cells based on $Sb_2Se_3$ is 3.2–9.2% (Choi et al., 2014; Leng et al., 2014; Zhou et al., 2015; Chen et al., 2017; Wen et al., 2018; Li et al., 2019). The efficiency of a $Sb_2Se_3$ solar cell is highly dependent on the physical properties of the base layer. To date, several methods were used for fabrication of $Sb_2Se_3$ films: vacuum-free (electrodeposition (Kim et al., 2017), successive ionic-layer adsorption and reaction (SILAR) (Phatan et al., 2004), chemical bath deposition (Kulkarni et al., 2015), spin-coating (Zhou et al., 2014), aerosol assisted chemical vapor deposition (Khan et al., 2018)), high and low vacuum methods (thermal evaporation (Liu et al., 2014; Kumar et al., 2019), vacuum evaporation (Mustafa et al., 2019), rapid thermal evaporation (Wang et al., 2017), vapor transport deposition (Liu et al., 2017), magnetron sputtering (Liang et al., 2017), close-spaced sublimation (Hutter et al., 2018)).

For all mentioned fabrication methods, the conductivity value of $Sb_2Se_3$ films is rather low $10^{-8} \div 10^{-6}$ (Ohm × cm)$^{-1}$. The efficiency of solar cell can be improved by increasing this value. The conductivity can be varied by the deviation from the stoichiometry of the films composition, owing to intrinsic point defects or by injection of extrinsic point defects, i.e. by impurities. Earlier in (Razykov et al., 2019), we reported characteristics of $Sb_2Se_3$ fabricated by CMBD from $Sb_2Se_3$ precursor. The conductivity of $Sb_xSe_y$ films fabricated by CMBD from separate Sb and Se precursors, depending on vapor phase mixture of the Sb/Se ratio, resulting in a deviation from stoichiometry of the films composition, is discussed in this paper.

* Corresponding author.
*E-mail address:* razykov@uzsci.net (T.M. Razykov).

https://doi.org/10.1016/j.solener.2021.10.012
Received 8 September 2021; Received in revised form 3 October 2021; Accepted 5 October 2021

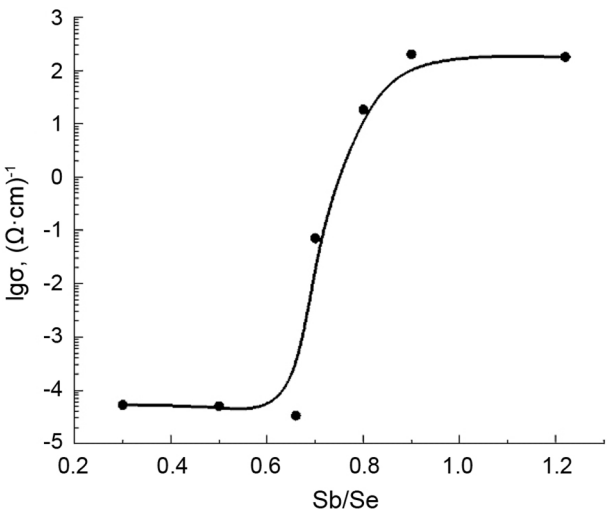


**Fig. 1.** The dependence of the conductivity of $Sb_xSe_y$ films on the Sb/Se ratio.

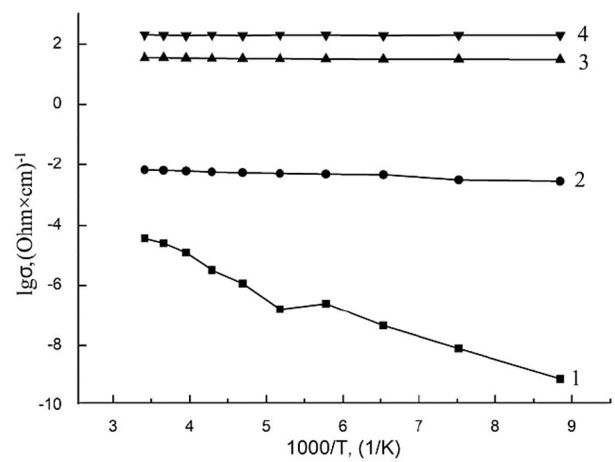


**Fig. 2.** The temperature dependence of the conductivity of samples fabricated at different Sb/Se ratios: 1) x = 0.5, 2) x = 0.7, 3) x = 0.8, 4) x = 0.9.

## 2. Experimental details

High purity of 99.999% Sb and Se granules were used as precursors. The sedimentation process of the $Sb_xSe_y$ films was carried out in the atmospheric pressure hydrogen flow and at substrate temperature of 500 °C. Soda-lime glass was cleaned using detergent, deionized water, acetone, and ethanol in sequence and used as substrate. The thickness was determined by microscope MIM-7.

At the Sb (800–900 °C) and Se (400–500 °C) evaporation temperatures, granules transfer into the vapor phase:

$$Sb(s) + 2Se(s) + H_2 = Sb(g) + Se_2(g) + H_2 \quad (1)$$

$Se_2$ (g) reacts with hydrogen and hydrogen selenide is formed:

$$Se_2(g) + 2H_2 = 2H_2Se(g) \quad (2)$$

Sb and Se atoms and $H_2Se$ molecules coverage the superficies of the substrate and $Sb_xSe_y$ films is formed as a consequence of their interplay:

$$3xSb(g) + ySe_2(g) + H_2Se(g) = 3Sb_xSe_y(s) + H_2 \quad (3)$$

The composition of $Sb_xSe_y$ films was controlled by changing the vapor phases mixture of Sb/Se ratio of Sb and Se (evaporated amount), which was varied by the molecular beam intensities of Sb and Se. Films thickness was 2–3 μm.

The electrical properties were measured by the 2-probe method. The contacts to the samples were made by evaporation of silver. The distance between the electrical contacts was 0.5 mm. Measurements of the films was carried out in the dark condition. Electrometer V7-30 was used for conductivity measurements. The type of conductivity of the films was determined by thermoprobe method.

## 3. Results and discussion

The dark conductivity of the $Sb_xSe_y$ films strongly depends on the Sb/Se ratio. The dependence of the conductivity of samples on Sb/Se ratio is presented in Fig. 1. It is seen that the conductivity is almost the same ($\sim 10^{-5}$ (Ohm × cm)$^{-1}$) for Sb/Se ratios in the range 0.3 ÷ 0.66. We have observed a drastically increasing of the conductivity from $10^{-5}$ (Ohm × cm)$^{-1}$ at Sb/Se ≥ 0.66 up to $10^2$ (Ohm × cm)$^{-1}$ at Sb/Se = 0.9 and it is almost unchanged until Sb/Se = 1.22. Moreover, we have established conversion of the type of the charge carriers, depending on the Sb/Se ratio. Samples demonstrated p-type conductivity at Sb/Se ≤ 0.7 and n-type conductivity at Sb/Se ≥ 0.8. From this behavior, we can see that there is "a tipping point" at Sb/Se = 0.7, which corresponds to the stoichiometric composition of $Sb_2Se_3$.

**Table 1**
The type of conductivity and the conductivity activation energy of samples fabricated at different Sb/Se ratios.

| Sb/Se | 0.5 | 0.7 | 0.8 | 0.9 |
|---|---|---|---|---|
| Type of conduc. | p | p | n | n |
| $E_a$, meV | 230; 140 | ~3 | ~3 | ~3 |

As seen from Fig. 2, the temperature-dependence of dark conductivity can be described by Arrhenius equation:

$$\sigma = \sigma_0 \exp (E_a/kT) \quad (4)$$

where σ is the dark conductivity, $\sigma_0$ is a constant, $E_a$ is the conductivity activation energy, k is the Boltzmann's constant and T is the absolute temperature. The dark conductivity increases with the temperature rise, for Sb/Se = 0.5, which is in good consent with the peculiarity of a semiconductor.

The activation energy is calculated to be about 230 meV for high temperature region and 140 meV for low temperature region. While samples fabricated at Sb/Se = 0.8 and 0.9 performed an "degenerated semiconductor" (the Fermi level is located in conduction band edge) behavior with an activation energy of ~3 meV (Table 1).

Activation energies $E_a$ = 230 meV and 140 meV correspond to "defect 2" and "defect 1", respectively, reported in (Hu et al., 2018). It is supposed that in Se-rich samples predominant defects are vacancy of antimony $V_{Sb}$ and antisite defect $Se_{Sb}$. While for Sb-rich samples predominant defects are vacancy of selenium $V_{Se}$ and interstitial antimony $Sb_i$. Se-rich films can be considered as compensated semiconductor with low conductivity containing acceptor ($V_{Sb}$) and donor ($Se_{Sb}$) levels. Sb-rich films can be considered as "degenerated semiconductor" with high conductivity and donor levels ($V_{Se}$ and $Sb_i$).

## 4. Conclusion

The conductivity of $Sb_xSe_y$ films was studied as a function of the vapor phase mixture of Sb and Se. By the precise control of the Sb/Se ratio we succeeded in obtaining stoichiometric $Sb_2Se_3$ films. It is also found out that we can control the conductivity by deliberately introducing the deviation from the stoichiometry. The conductivity was varied in the wide range of $10^{-5}$–$10^2$ (Ohm × cm)$^{-1}$ and samples had p- and n-type of conductivity depending on Sb/Se ratio. It is supposed that in Se-rich samples predominant defects are vacancy of antimony $V_{Sb}$ and antisite defect $Se_{Sb}$. While for Sb-rich samples predominant defects are vacancy of selenium $V_{Se}$ and interstitial antimony $Sb_i$.

## Declaration of Competing Interest

The authors declare that they have no known competing financial interests or personal relationships that could have appeared to influence the work reported in this paper.

## Acknowledgements

This work was supported by the Program for Basic Research of Uzbekistan Academy of Sciences.

## References

Chen, C., Wang, L., Gao, L., Nam, D., Li, D., Li, K., Zhao, Y., Ge, C., Cheong, H., Liu, H., Song, H., Tang, J., 2017. 6.5% Certified efficiency $Sb_2Se_3$ solar cells using PbS colloidal quantum dot film as hole-transporting layer. ACS Energy Lett. 2 (9), 2125–2132.

Choi, Y.C., Mandal, T.N., Yang, W.S., et al., 2014. $Sb_2S_3$ sensitized inorganic-organic heterojunction solar cells fabricated using a singlesource precursor. Angew. Chem. Int. Ed. 126 (5), 1353–1357.

Hongwei, L., Jianjun, C., Zuojun, T., et al., 2019. Review of recent progress in antimony chalcogenide-based solar cells: materials and devices. Sol. RRL 3 (6), 1900026. https://doi.org/10.1002/solr.v3.610.1002/solr.201900026.

Hu, X., Tao, J., Weng, G., et al., 2018. Investigation of electrically-active defects in $Sb_2Se_3$ thin-film solar cells with up to 5.91% efficiency via admittance spectroscopy. Sol. Energy Mater. Sol. Cells 186, 324–329.

Hutter, O.S., Phillips, L.J., Yates, P.J., et al., 2018. CSS Antimony selenide film morphology and high efficiency PV devices. In: IEEE 7th World Conference on Photovoltaic Energy Conversion (WCPEC) (A Joint Conference of 45th IEEE PVSC, 28th PVSEC & 34th EU PVSEC). IEEE, pp. 0027–0031.

Khan, M.D., Aamir, M., Sohail, M., Sher, M., Akhtar, J., Malik, M.A., Revaprasadu, N., 2018. Novel single source precursor for synthesis of $Sb_2Se_3$ nanorods and deposition of thin films by AACVD: photo-electrochemical study for water reduction catalysis. Sol. Energy 169, 526–534.

Kim, Y.B., Jeong, M., Do, H.W., Cho, H.K., Lee, J.Y., 2017. Crystal growth direction-controlled antimony selenide thin film absorbers produced using an electrochemical approach and intermediate thermal treatment. Sol. Energy Mater. Sol. Cells 172, 11–17.

Kulkarni, A., Arote, S., Pathan, H., et al., 2015. $Sb_2Se_3$ sensitized heterojunction solar cells, Materials for Renewable and Sustainable. Energy 4, 1–15.

Kumar, V., Artegiani, E., Kumar, A., et al., 2019. Effects of post-deposition annealing and copper inclusion in superstrate $Sb_2Se_3$ based solar cells by thermal evaporation. Sol. Energy 193, 452–457.

Leng, M., Luo, M., Chen, C., Qin, S., Chen, J., Zhong, J., Tang, J., 2014. Selenization of $Sb_2Se_3$ absorber layer: An efficient step to improve device performance of CdS/$Sb_2Se_3$ solar cells. Appl. Phys. Lett. 105 (8), 083905. https://doi.org/10.1063/1.4894170.

Li, Z., Liang, X., Li, G., Liu, H., Zhang, H., Guo, J., Chen, J., Shen, K., San, X., Yu, W., Schropp, R.E.I., Mai, Y., 2019. 9.2%-efficient core-shell structured antimony selenide nanorod array solar cells. Nat. Commun. 10 (1) https://doi.org/10.1038/s41467-018-07903-6.

Liang, G.-X., Zhang, X.-H., Ma, H.-L., Hu, J.-G., Fan, B., Luo, Z.-K., Zheng, Z.-H., Luo, J.-T., Fan, P., 2017. Facile preparation and enhanced photoelectrical performance of $Sb_2Se_3$ nano-rods by magnetron sputtering deposition. Sol. Energy Mater. Sol. Cells 160, 257–262.

Liu, X., Chen, J., Luo, M., Leng, M., Xia, Z., Zhou, Y., Qin, S., Xue, D.-J., Lv, L., Huang, H., Niu, D., Tang, J., 2014. Thermal evaporation and characterization of $Sb_2Se_3$ thin film for substrate $Sb_2Se_3$/CdS solar cells. ACS Applied Materials Interfaces 6 (13), 10687–10695.

Liu, X., Xiao, X., Yang, Y.e., Xue, D.-J., Li, D.-B., Chen, C., Lu, S., Gao, L., He, Y., Beard, M.C., Wang, G., Chen, S., Tang, J., 2017. Enhanced $Sb_2Se_3$ solar cell performance through theory-guided defect control. Prog. Photovolt.: Res. Appl. 25 (10), 861–870.

Mamta, Y., Singh, K.K.M., et al., 2021. A review on properties, applications, and deposition techniques of antimony selenide. Sol. Energy Mater. Sol. Cells 230, 111223.

Mavlonov, A., Razykov, T., Raziq, F., Gan, J., Chantana, J., Kawano, Y.u., Nishimura, T., Wei, H., Zakutayev, A., Minemoto, T., Zu, X., Li, S., Qiao, L., 2020. A review of $Sb_2Se_3$ photovoltaic absorber materials and thin-film solar cells. Sol. Energy 201, 227–246.

Mustafa, F.I., Gupta, S., Goyal, N., et al., 2019. Effect of temperature on the optical parameter of amorphous Sb-Se thin films. J. Optoelectron. Adv. Mater. 11 (12), 2019–2023.

Pathan, H.M., Lokhande, C.D., 2004. Deposition of metal chalcogenide thin films by successive ionic layer adsorption and reaction (SILAR) method. Bull. Mater. Sci. 27 (2), 85–111.

Razykov, T.M., Shukurov, A.K., Kuchkarov, K.M., Ergashev, B.A., Khurramov, R.R., Bekmirzoyev, J.G., Mavlonov, A.A., 2019. Morphological and structural characteristics of $Sb_2Se_3$thin films fabricated by chemical molecular beam deposition. Appl. Solar Energy 55 (6), 376–379.

Wang, L., Li, D.-B., Li, K., Chen, C., Deng, H.-X., Gao, L., Zhao, Y., Jiang, F., Li, L., Huang, F., He, Y., Song, H., Niu, G., Tang, J., 2017. Stable 6%-efficient $Sb_2Se_3$ solar cells with a ZnO buffer layer. Nat. Energy 2 (4). https://doi.org/10.1038/nenergy.2017.46.

Wen, X., Chen, C., Lu, S., Li, K., Kondrotas, R., Zhao, Y., Chen, W., Gao, L., Wang, C., Zhang, J., Niu, G., Tang, J., 2018. Vapor transport deposition of antimony selenide thin film solar cells with 7.6% efficiency. Nat. Commun. 9 (1) https://doi.org/10.1038/s41467-018-04634-6.

Zhou, Y., Leng, M., Xia, Z., 2014. Solution-processed antimony selenide heterojunction solar cells. Adv. Energy Mater. 4 (8), 1301846.

Zhou, Y., Wang, L., Chen, S., Qin, S., Liu, X., Chen, J., Xue, D.-J., Luo, M., Cao, Y., Cheng, Y., Sargent, E.H., Tang, J., 2015. Thin-film $Sb_2Se_3$ photovoltaics with oriented one-dimensional ribbons and benign grain boundaries. Nat. Photonics 9 (6), 409–415.